

An efficient inverse approach for reconstructing time- and space-dependent heat flux of participating medium

Shuang-Cheng Sun(孙双成), Guang-Jun Wang(王广军), Hong Chen(陈红)

Citation: Chin. Phys. B . 2020, 29(11): 110202 . **doi:** 10.1088/1674-1056/aba608
Journal homepage: http://cpb.iphy.ac.cn; http://iopscience.iop.org/cpb

What follows is a list of articles you may be interested in

Factorization method for inverse obstacle scattering problem in three-dimensional planar acoustic waveguides

Xue Qin(秦雪)

Chin. Phys. B . 2018, 27(10): 100203 . **doi:** 10.1088/1674-1056/27/10/100203

Accurate reconstruction of the optical parameter distribution in participating medium based on the frequency-domain radiative transfer equation

Yao-Bin Qiao(乔要宾), Hong Qi(齐宏), Fang-Zhou Zhao(赵方舟), Li-Ming Ruan(阮立明)

Chin. Phys. B . 2016, 25(12): 120201 . **doi:** 10.1088/1674-1056/25/12/120201

Direction-of-arrival estimation for co-located multiple-input multiple-output radar using structural sparsity Bayesian learning

Wen Fang-Qing, Zhang Gong, Ben De

Chin. Phys. B . 2015, 24(11): 110201 . **doi:** 10.1088/1674-1056/24/11/110201

Designing shielded radio-frequency phased-array coils for magnetic resonance imaging

Xu Wen-Long, Zhang Ju-Cheng, Li Xia, Xu Bing-Qiao, Tao Gui-Sheng

Chin. Phys. B . 2013, 22(1): 010203 . **doi:** 10.1088/1674-1056/22/1/010203

Relevance vector machine technique for the inverse scattering problem

Wang Fang-Fang,Zhang Ye-Rong

Chin. Phys. B . 2012, 21(5): 050204 . **doi:** 10.1088/1674-1056/21/5/050204

An efficient inverse approach for reconstructing time- and space-dependent heat flux of participating medium*

Shuang-Cheng Sun(孙双成)[1,2,†], Guang-Jun Wang(王广军)[1,2], and Hong Chen(陈红)[1,2]

[1] School of Energy and Power Engineering, Chongqing University, Chongqing 400044, China
[2] Key Laboratory of Low-grade Energy Utilization Technologies and Systems, Ministry of Education, Chongqing University, Chongqing 400044, China

(Received 4 May 2020; revised manuscript received 26 May 2020; accepted manuscript online 15 July 2020)

The decentralized fuzzy inference method (DFIM) is employed as an optimization technique to reconstruct time- and space-dependent heat flux of two-dimensional (2D) participating medium. The forward coupled radiative and conductive heat transfer problem is solved by a combination of finite volume method and discrete ordinate method. The reconstruction task is formulated as an inverse problem, and the DFIM is used to reconstruct the unknown heat flux. No prior information on the heat flux distribution is required for the inverse analysis. All retrieval results illustrate that the time- and space-dependent heat flux of participating medium can be exactly recovered by the DFIM. The present method is proved to be more efficient and accurate than other optimization techniques. The effects of heat flux form, initial guess, medium property, and measurement error on reconstruction results are investigated. Simulated results indicate that the DFIM is robust to reconstruct different kinds of heat fluxes even with noisy data.

Keywords: decentralized fuzzy inference, surface heat flux reconstruction, inverse heat transfer problem, participating medium

PACS: 02.30.Zz, 45.10.Db, 44.40.+a, 43.20.Ye **DOI:** 10.1088/1674-1056/aba608

1. Introduction

Accurate measurement of time- and space-dependent heat flux is significant to numerous scientific researches and engineering applications, such as glass pressing,[1,2] combustion diagnosis,[3,4] tumor thermal therapy,[5,6] hot rolling,[7,8] to name a few.[9–13] Direct measurement of transient heat flux is a challenging task in many industry fields. For instance, the time- and space-dependent heat flux on the wall subjected to fire is difficult to identify in a combustion chamber. The transient heat flux distribution cannot be directly measured in a control rod of nuclear power plant. Similar measurement problems often encountered in modern turbomachinery and spacecraft thermal protection system.[14] Inverse analysis plays a critical role in such circumstances, in which the transient heat flux is indirectly determined by solving inverse heat transfer problems (IHTPs).

IHTP is mathematically ill-posed in the sense that the uniqueness and existence of solution cannot be ensured.[15–18] To date, lots of optimization techniques with anti-ill-posedness have been developed for solving IHTPs. In general, the theoretical approaches can be classified into two categories: stochastic algorithms and deterministic methods. Stochastic algorithm is easy for computer programming and independent on initial guess. Meanwhile, quite a few candidates can be dealt with in parallel at each iteration and a global optimum can be achieved. Various inverse problems have been solved by stochastic algorithms. For example, Qi *et al.*[19–21] used particle swarm optimization (PSO) algorithm to identify the physical parameters of participating medium and optimize the geometric shape of radiative enclosure. Li *et al.*[22] applied ant colony optimization (ACO) algorithm to determine the heat source position by solving IHTPs. Many other intelligent algorithms such as differential evolution (DE), artificial neural networks (ANN), and social spider optimization (SSO) have also been successfully used for solving IHTPs.[23–28] However, only a few parameters can be concurrently identified by stochastic algorithms. It is difficult to solve complex identification tasks (such as the reconstruction of transient heat flux) using stochastic algorithms.

Determine methods are widely used to solve IHTPs for their high computational accuracy and strong stability.[29,30] Yang *et al.*[31] applied conjugate gradient method (CGM) to determine the time- and space-dependent heat flux of brake system, in which the time-resolved temperature distribution measured within the disc was employed as measurement signals. Zhu *et al.*[32] employed CGM to reconstruct the transient heat flux on the high-temperature wall of an engine, and the accuracy of reconstruction model was verified by experimental tests. Cui *et al.*[33] used Levenberg–Marquardt (L–M) method to reconstruct the parameters of space-dependent heat flux. Sun *et al.*[34] introduced sequential quadratic programming (SQP) algorithm to reconstruct the transient heat flux of participating media. The SQP algorithm achieved better reconstruction results than CGM and L–M method. Excellent

*Project supported by the Natural Science Foundation of Chongqing (CSTC, Grant No. 2019JCYJ-MSXMX0441).
†Corresponding author. E-mail: scsun@cqu.edu.cn
© 2020 Chinese Physical Society and IOP Publishing Ltd

reconstruction results of transient heat fluxes were retrieved using gradient-based methods. However, the optimization process is time-consuming in the sense that the gradient distribution is difficult to obtain, especially for multi-dimensional coupled heat transfer problems.

Fuzzy inference method (FIM) is widely applied to solve ill-posed problems.[35] The inference rule of FIM simulates human thinking using mathematic method. A variety of fuzzy control and recognition problems have been solved by using FIM. Wang *et al.*[36,37] proposed a decentralized FIM (DFIM) to reconstruct the surface heat flux and boundary shape of heat transfer system. Retrieval results indicated that the DFIM was more robust than other inverse methodologies such as CGM, GA, and dynamic matrix control (DMC). Sun *et al.*[38] developed three improved DFIMs to reconstruct the time-dependent surface heat flux of one-dimensional (1D) participating medium. However, to the best knowledge of the authors, the application of DFIM for reconstructing the time- and space-dependent heat flux of participating medium has not yet been investigated. In this study, the DFIM is introduced to determine the transient heat flux of participating medium by solving inverse coupled radiative and conductive heat transfer (CRCHT) problems. The remainder of this work is organized as follows. In Section 2, the forward model concerning on CRCHT in 2D participating medium is described. In Section 3, the fundamentals of DFIM are introduced in detail and the flowchart of DFIM for solving inverse CRCHT problems is provided. In Section 4, the time- and space-dependent heat flux of participating medium is reconstructed. Meanwhile, the effects of heat flux form, initial guess, medium property and measurement error on estimation results are studied in this section. The main conclusions are presented in Section 5.

2. Forward model

The transient CRCHT in 2D participating medium is considered in this section. As illustrated in Fig. 1, the medium walls are assumed to be diffuse and opaque. All boundaries are subjected to Cauchy boundary conditions. Meanwhile, the left wall is irradiated by an external heat source. The energy equation governing the CRCHT problem can be expressed as[39]

$$\rho c_{\mathrm{p}} \frac{\partial T}{\partial t} = \nabla \cdot (\lambda \nabla T) - \nabla \cdot \boldsymbol{q}^{\mathrm{r}}, \tag{1}$$

where ρ, c_{p}, and λ indicate the density, specific heat, and thermal conductivity, respectively. T represents temperature and t represents time. $\boldsymbol{q}^{\mathrm{r}}$ is the radiative heat flux expressed as follows:

$$\nabla \cdot \boldsymbol{q}^{\mathrm{r}} = \kappa_{\mathrm{a}} \left[4\pi I_{\mathrm{b}}(s) - \int_{4\pi} I(s, \boldsymbol{\Omega}) \, \mathrm{d}\Omega \right], \tag{2}$$

where κ_{a} represents the absorption coefficient. $I_{\mathrm{b}} = n^2 \sigma T^4 / \pi$ is the radiative intensity of blackbody at temperature T, n indicates the refractive index, σ is the Stefan–Boltzmann constant. The spatial position and transfer direction are denoted by s and $\boldsymbol{\Omega}$, respectively.

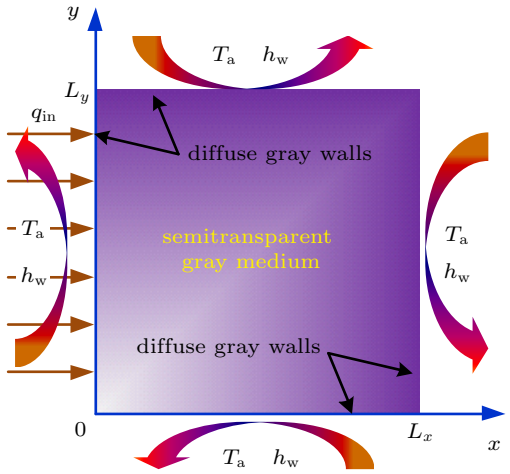


Fig. 1. Schematic diagram of CRCHT in 2D participating medium.

The initial and boundary conditions can be given as

$$T(s,t)|_{t=0} = T_0, \tag{3}$$

$$q^{\mathrm{r}}_{\mathrm{w1}} - \lambda \left. \frac{\partial T}{\partial x} \right|_{x=0} = q_{\mathrm{in}} + h_{\mathrm{w}} (T_{\mathrm{a}} - T_{\mathrm{w1}}), \tag{4}$$

$$q^{\mathrm{r}}_{\mathrm{w2}} + \lambda \left. \frac{\partial T}{\partial x} \right|_{x=L_x} = h_{\mathrm{w}} (T_{\mathrm{a}} - T_{\mathrm{w2}}), \tag{5}$$

$$q^{\mathrm{r}}_{\mathrm{w3}} - \lambda \left. \frac{\partial T}{\partial y} \right|_{y=0} = h_{\mathrm{w}} (T_{\mathrm{a}} - T_{\mathrm{w3}}), \tag{6}$$

$$q^{\mathrm{r}}_{\mathrm{w4}} + \lambda \left. \frac{\partial T}{\partial y} \right|_{y=L_y} = h_{\mathrm{w}} (T_{\mathrm{a}} - T_{\mathrm{w4}}), \tag{7}$$

where T_0 represents the initial temperature. q_{in} indicates the incident heat flux. T_{a} denotes the ambient temperature. h_{w} is the convective heat transfer coefficient. The subscripts w1, w2, w3, and w4 represent the left, right, bottom, and top walls of the medium, respectively.

The radiative intensity in Eq. (2) can be calculated by solving the radiative transfer equation (RTE)[39]

$$\frac{\mathrm{d}I(s, \boldsymbol{\Omega})}{\mathrm{d}s} = -\kappa_{\mathrm{e}} I(s, \boldsymbol{\Omega}) + \kappa_{\mathrm{a}} I_{\mathrm{b}}(s) + \frac{\kappa_{\mathrm{s}}}{4\pi} \int_{4\pi} I(s, \boldsymbol{\Omega}') \, \Phi(\boldsymbol{\Omega}', \boldsymbol{\Omega}) \, \mathrm{d}\Omega', \tag{8}$$

where κ_{e} represents the extinction coefficient, κ_{s} represents the scattering coefficient, and $\Phi(\boldsymbol{\Omega}', \boldsymbol{\Omega})$ denotes the scattering phase function.

The surfaces of the medium are assumed to be opaque, diffuse and gray walls in this study. Hence, the boundary condition for the RTE can be given as

$$I_{\mathrm{w}} = \varepsilon_{\mathrm{w}} I_{\mathrm{b,w}} + \frac{1 - \varepsilon_{\mathrm{w}}}{\pi} \int_{\boldsymbol{n}_{\mathrm{w}} \cdot \boldsymbol{\Omega} < 0} I_{\mathrm{w}}(\boldsymbol{\Omega}) \, |\boldsymbol{n}_{\mathrm{w}} \cdot \boldsymbol{\Omega}| \, \mathrm{d}\Omega, \quad \boldsymbol{n}_{\mathrm{w}} \cdot \boldsymbol{\Omega} > 0, \tag{9}$$

where ε_w indicates the wall emissivity of the medium. The normal vector is denoted by $\boldsymbol{n}_w$.

The finite volume method (FVM) and discrete ordinate method (DOM) are applied to solve the energy equation and RTE, respectively.[25,39] To test the reliability of the FVM–DOM solution for solving CRCHT problems, a typical simulation case is considered. The parameters are taken as the same values with those in Ref. [40] as listed in Table 1.

Table 1. Parameters in the verification case.

Parameter	L_x/m	L_y/m	λ/W·m^{-1}·K^{-1}	κ_a/m^{-1}	κ_s/m^{-1}	n	ε_w	Φ
Value	1.0	1.0	2.268, 22.68, 226.8	1.0	0.0	1.0	1.0	1.0

The simulation results are in good agreement with Ref. [40] solved by a combination of lattice Boltzmann method and DOM (see Fig. 2), which demonstrates the reliability of the present solution.

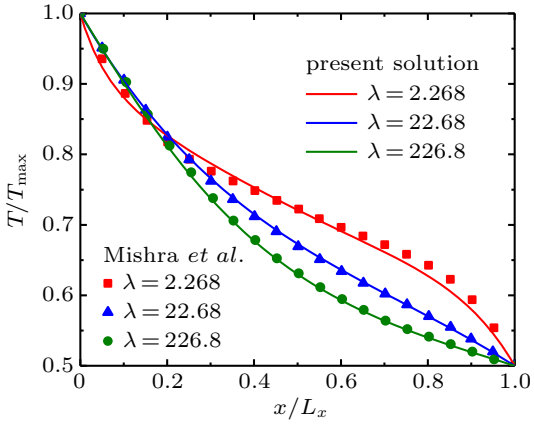


Fig. 2. Verification of the FVM–DOM solution for solving CRCHT problem in 2D participating medium.

3. Inverse model

In this study, the incident heat flux on the left wall will be reconstructed without prior information. The time-dependent temperature on the left wall is employed as measurement signals. The reconstruction task is formulated as an inverse problem. The DFIM is applied to determine the time- and space-dependent heat flux by solving inverse CRCHT problem.

Fuzzy inference unit (FIU) is the core section of DFIM and is formulated according to expert experience. For the reconstruction of transient heat flux, the surface temperature is served as input for the inverse analysis. The input signal can be expressed as:

$$e_{m,n} = T_{m,n,\mathrm{rec}} - T_{m,n,\mathrm{mea}}, \tag{10}$$

where e represents the input signal for the fuzzy inference unit. The subscripts m and n indicate the m-th measurement time and n-th measurement position, respectively. The subscript rec denotes the simulated boundary temperature using reconstructed heat flux. The subscript mea denotes the measured temperature signal.

The main intention of fuzzy inference unit is to generate an effective heat flux compensation $u_{m,n}$ on the basis of input signal $e_{m,n}$. The ranges of input and output are denoted by $[-r_i, r_i]$ and $[-r_o, r_o]$, respectively. The input and output domains are linearly divided into 7 fuzzy subsets in the present research, and they are denoted by $\{A_1, A_2, \ldots, A_7\}$ and $\{B_1, B_2, \ldots, B_7\}$ respectively. Meanwhile, the fuzzy sets A and B are marked as NB, NM, NS, ZO, PS, PM, and PB. The membership function is defined by isosceles triangle, and hence the membership value γ can be obtained according to the following Fig. 3.

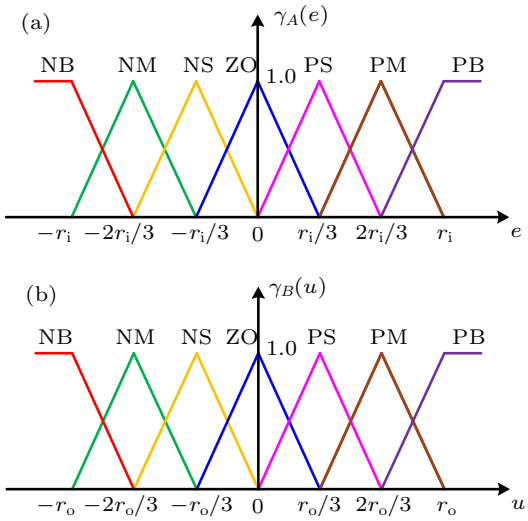


Fig. 3. Membership functions of (a) fuzzy input set and (b) fuzzy output set.

For the CRCHT problem, the bigger the incident heat flux is, the higher the measured boundary temperature will be. Thus, if the reconstructed boundary temperature is less than the measured temperature (*i.e.*, $e_{m,n} < 0$), which means the reconstructed surface heat flux is less than the exact one, thereby a positive compensation should be provided for the optimization parameter. In contrast, a negative compensation is required for the heat flux reconstruction when $e_{m,n} > 0$. Meanwhile, the absolute value of requisite compensation increases with the increment of $|e_{m,n}|$. Thus, the fuzzy rules between input and output can be established as shown in Table 2.

Table 2. Fuzzy rules of DFIM.

$e_{m,n}$	NB	NM	NS	ZO	PS	PM	PB
$u_{m,n}$	PB	PM	PS	ZO	NS	NM	NB

The Mamdani maximum–minimum inference method is employed as the inference engine, which can be given as

follows:[41]

$$\gamma_B(u_{m,n}) = \max_{l=1}^{7}\left\{\min\left[\gamma_{A_l}(e_{m,n}),\ \gamma_{B_l}(u_{m,n})\right]\right\}, \tag{11}$$

where $\gamma_{A_l}(e_{m,n})$ and $\gamma_{B_l}(u_{m,n})$ represent the membership values of input signal $e_{m,n}$ and output variable $u_{m,n}$ corresponding to fuzzy sets A_l and B_l, and they are determined according to Figs. 3(a) and 3(b), respectively.

The retrieval result of fuzzy inference unit is a fuzzy variable which cannot be directly used for the update of optimization parameters. Hence, a defuzzifier is required to produce an effective inference results. The barycenter method is used as the defuzzifier, which is expressed as[42]

$$d_{m,n} = \frac{\int_{-r_o}^{r_o}\gamma_B(u_{m,n})\,u_{m,n}\,\mathrm{d}u}{\int_{-r_o}^{r_o}\gamma_B(u_{m,n})\,\mathrm{d}u}, \tag{12}$$

where d indicates the final output of FIU.

The measured temperature signals at different time and positions provide different influence on the time- and space-dependent heat flux, which means the inference result of each fuzzy inference unit will produce different influence on the reconstruction parameter. Weighting mechanisms are employed to coordinate the influence of different measurement signals. The weighting factor is generated by sensitivity method in this study. The weighting factor of the measured temperature at m-th time and n-th position with respect to the reconstructed heat flux at i-th time and j-th position is defined as

$$\alpha_{m,n,i,j} = \frac{\Psi_{q_{i,j}}(T_{m,n})}{\sum_{m=1}^{NT}\sum_{n=1}^{NP}\Psi_{q_{i,j}}(T_{m,n})}, \tag{13}$$

where the numbers of measurement time and position are denoted by NT and NP, respectively. $\Psi_{q_{i,j}}(T_{m,n})$ represents the sensitivity coefficient of $T_{m,n}$ with respect to $q_{i,j}$, it can be calculated by

$$\Psi_{q_{i,j}}(T_{m,n}) = \frac{T_{m,n}(q_{i,j}+\delta q_{i,j}) - T_{m,n}(q_{i,j}-\delta q_{i,j})}{2\delta q_{i,j}}, \tag{14}$$

where δ is a fluctuation which is taken as $\delta = 0.005$ in the present research. $i = 1, 2, \ldots, NI$; $j = 1, 2, \ldots, NJ$; NI and NJ denote the number of reconstruction time and position, respectively.

Thus, the boundary heat flux to be reconstructed can be generated as follows:

$$q_{i,j}^{k} = q_{i,j}^{k-1} + \alpha_{m,n,i,j}^{k} d_{m,n}^{k}, \tag{15}$$

where the superscript k indicates the k-th iteration. The fuzzy inference system of DFIM is illustrated in Fig. 4.

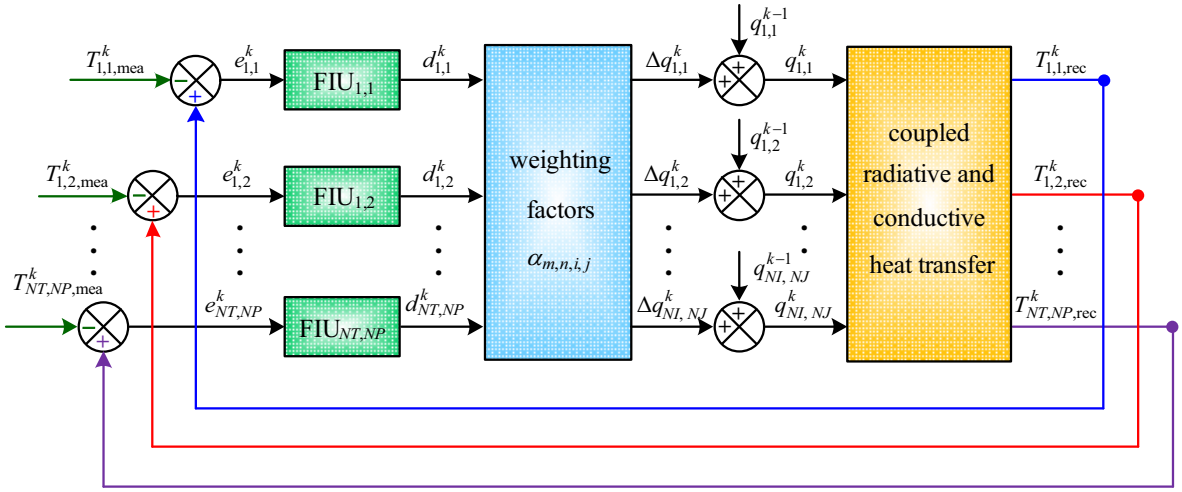


Fig. 4. Fuzzy inference system of DFIM.

However, the retrieval result of fuzzy inference system is limited by the output domain, and thereby an effective output for the update of reconstruction parameter is difficult to generate in the above DFIM. To overcome the drawback of the conventional DFIM, an amplification coefficient is introduced and the reconstruction parameter is updated by

$$q_{i,j}^{k} = q_{i,j}^{k-1} + \chi^{k}\alpha_{m,n,i,j}^{k} d_{m,n}^{k}, \tag{16}$$

where χ is the amplification factor. In the early reconstruction process, a large compensation is necessary for the heat flux update to accelerate the optimization velocity. In contrast, a small compensation conducts careful reconstruction works, which is valuable in the last optimization stage. Thus, an iteration-dependent amplification factor is applied to control the reconstruction compensation, which is given by

$$\chi^{k} = \begin{cases} \dfrac{(k-k_0)^2}{k_0^2}\chi_0 + \chi_{\min}, & k \le k_0, \\ \chi_{\min}, & k > k_0, \end{cases} \tag{17}$$

where χ_0 and $\chi_{\min}$ represent the specified and the minimum

values of amplification factor, respectively. k_0 indicates a specified iteration number.

Moreover, a linearly decreasing output domain is employed to control the inference output. The iteration-dependent output range is defined as

$$r_{\mathrm{o}} = r_{\mathrm{o,max}} - \frac{k}{k_{\max}} \times \left(r_{\mathrm{o,max}} - r_{\mathrm{o,min}}\right), \tag{18}$$

where the maximum and minimum output ranges are represented by $r_{\mathrm{o,max}}$ and $r_{\mathrm{o,min}}$, respectively. $k_{\max}$ is the maximum iteration number.

The iterative optimization stops until one of the following stop criteria is satisfied:

$$k = k_{\max}, \tag{19}$$

$$F_{\mathrm{obj}} = \sum_{m=1}^{NT} \sum_{n=1}^{NP} \left(T_{m,n,\mathrm{rec}} - T_{m,n,\mathrm{mea}}\right)^2 < \varepsilon, \tag{20}$$

where F_{obj} represents the objective function, ε is the iterative accuracy. The flowchart of the DFIM for reconstructing the time- and space-dependent heat flux of participating medium is shown in Fig. 5. It is worth noting that the weight factors are calculated before iterative optimization because the sensitive tendency of measurement signals with respect to reconstruction parameters remains unchanged at each iteration.

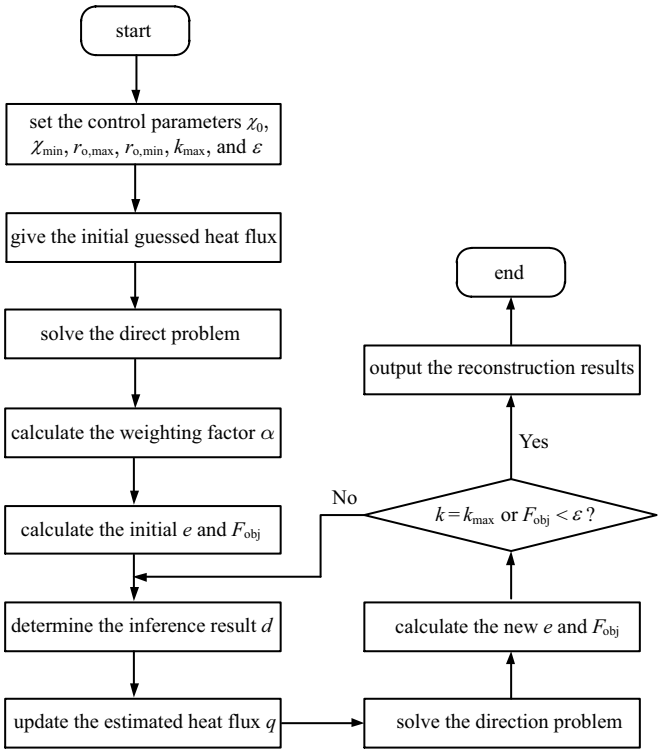


Fig. 5. Flowchart of DFIM for reconstructing time- and space-dependent heat flux.

4. Results and discussion

This research aims to reconstruct the time- and space-dependent heat flux of 2D participating medium using DFIM. The time-resolved temperature on the left boundary is employed as measurement signals. Since noisy data is inevitable in practical measurement, random standard deviations are added to the boundary temperature. Hence, the measurement signal can be expressed as

$$T_{m,n,\mathrm{mea}} = T_{m,n,\mathrm{exa}} + \sigma\varsigma, \tag{21}$$

where the subscript exa indicates the simulated boundary temperature by using exact heat flux. σ represents the standard deviation of measurement signal. ς is a random value of normal distribution with zero mean and unit standard deviation.

To assess the performance of DFIM, the relative error is introduced and expressed as

$$\varepsilon_{\mathrm{rel}} = \begin{cases} \dfrac{|q_{\mathrm{est}} - q_{\mathrm{exa}}|}{q_{\mathrm{exa}}} \times 100\%, & q_{\mathrm{exa}} \neq 0, \\ \dfrac{|q_{\mathrm{est}} - q_{\mathrm{exa}}|}{q_{\mathrm{ave}}} \times 100\%, & q_{\mathrm{exa}} = 0, \end{cases} \tag{22}$$

where q_{rec} represents the reconstructed heat flux of DFIM, q_{exa} is the exact value of incident heat flux, q_{ave} indicates the average value of q_{exa}.

Each case is implemented using the FORTRAN code, and the programs run on an Intel®Core™ i5-8400 CPU.

4.1. Reconstruction of the time- and space-dependent heat flux

The participating medium considered in this study is gray medium with size of $L_x \times L_y = 0.01 \times 0.01$ m^2. The ambient temperature is set as $T_{\mathrm{a}} = 300$ K. The convective heat transfer coefficient is $h_{\mathrm{w}} = 7$ W/(m^2·K). The absorption and scattering coefficients of the 2D participating medium are set as $\kappa_{\mathrm{a}} = 10$ m^{-1} and $\kappa_{\mathrm{s}} = 10$ m^{-1}, respectively. The refractive index of the medium is set as $n = 1.5$. The other physical parameters of the medium are taken as same values with those in Section 2. The sampling time step is set as $\Delta t = 0.1$ s, and the number of sampling time and position is taken as $NT = 100$ and $NP = 20$, respectively. The maximum iteration number is set as $k_{\max} = 1000$, and the convergence accuracy of DFIM is taken as $\varepsilon = 10^{-4}$.

The time- and space-dependent heat flux is given as follows:

$$\begin{aligned} \mathrm{Q1}: q(y,t) \;=\; & 10000 + 30000\left(1 - \mathrm{e}^{-0.8t}\right) \\ & + 15000 \sin t \sin\left(0.5\pi Y\right), \end{aligned} \tag{23}$$

where $Y = y/L_y$ denotes the dimensionless ordinate. The DFIM is applied to reconstruct the heat flux Q1 and the initial guessed values are taken as $q(y,t) = 10000$ W/m^2. The exact and reconstructed heat flux distributions are illustrated in Fig. 6.

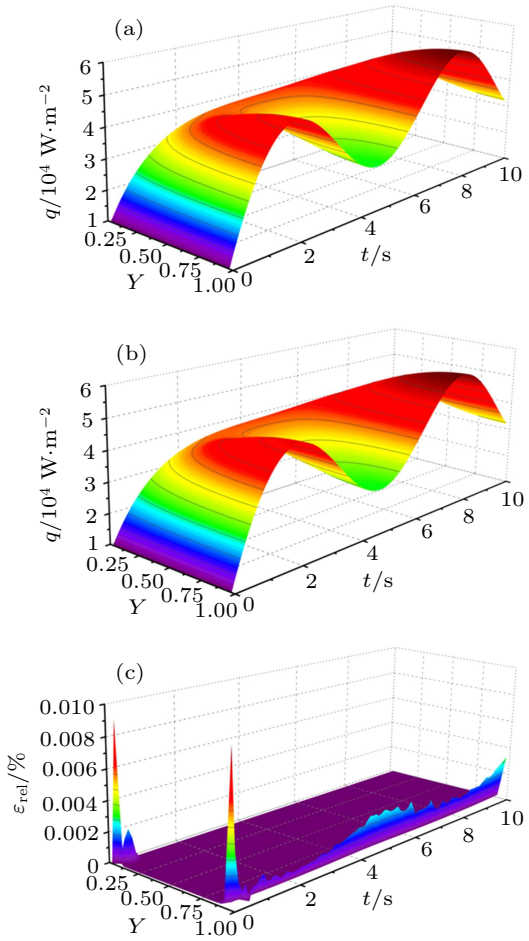


Fig. 6. Reconstruction results of heat flux Q1 using DFIM. (a) Exact distribution, (b) reconstructed results, and (c) relative error distribution.

As shown in the figure, the retrieval results of DFIM are in good agreement with exact values. The maximum relative error of the reconstruction result is less than 0.01%, which demonstrates the time- and space-dependent heat flux of 2D participating medium can be accurately recovered using the DFIM.

To show the performance of the present DFIM for reconstructing the time- and space-dependent heat flux, the retrieval results including computational accuracy and efficiency are compared with those obtained by other inverse techniques such as SQP algorithm, CGM, L–M method, PSO, and GA. The initial guessed heat flux and stop criteria are taken as the same values as in DFIM, SQP algorithm, CGM, and L–M methods. Since swarm diversity is of great significance to intelligent algorithms, the initial heat flux is randomly produced in the searching domain $[0, 10^5]$ in PSO algorithm and GA. Meanwhile, the population size is set as $M = 30$. The maximum iteration number and convergence accuracy of PSO algorithm and GA are taken as $k_{\max} = 10000$ and $\varepsilon = 10^{-4}$, respectively. The other reconstruction parameters are set as the same values for all optimization techniques.

Table 3 lists the retrieval results of different optimization techniques. As illustrated, the transient heat flux can be accurately recovered by DFIM, SQP algorithm, CGM, and L–M methods. The present DFIM achieves better performance than other inverse methods in terms of reconstruction accuracy and efficiency. The retrieval relative errors of PSO and GA are much larger than above deterministic methodologies, which is mainly due to the stochastic characteristic of swarm intelligent algorithms.

Table 3. Reconstruction results of time- and space-dependent heat flux using different optimization techniques.

Optimization technique	Average relative error/%	Maximum relative error/%	Iteration number	Computational time/h
DFIM	0.0002	0.0092	46	0.3
SQP	0.0003	0.0229	306	86.2
CGM	0.0010	0.1341	698	153.3
L-M	0.0015	0.2056	717	172.9
PSO	44.8900	287.7838	10000	23.8
GA	59.2025	392.2087	10000	36.1

4.2. Effect of heat flux form

Since the practical heat fluxes irradiated on the participating medium are significantly different in various engineering applications, different kinds of incident heat fluxes are investigated. The functional forms of heat flux are given as follows:

$$\text{Q2}: \ q(y,t) = 3\times10^4 + 2.3\times10^4 \sin\left[Y^2+t^2\right]^{1/2}, \tag{24}$$

$$\text{Q3}: \ q(y,t) = 4\times10^4 + 2.5\times10^4 \sin(2\pi Y)\cos(0.2\pi t), \tag{25}$$

$$\text{Q4}: \ q(y,t) = 3\times10^4 + 500[(5Y)^2 + (0.5t)^2 - 10\cos(10\pi Y) - 10\cos(0.2\pi t)], \tag{26}$$

$$\text{Q5}: \ q(y,t) = 5\times10^4 - 2\times10^4[\sin(\pi Y)\sin^{20}(\pi Y^2) + \sin(0.1\pi t)\sin^{20}(0.02\pi t^2)]. \tag{27}$$

As shown in Figs. 7–10, all the above heat fluxes are precisely reconstructed by the DFIM. Table 4 illustrates the retrieval relative error and reconstruction time of different kinds of heat fluxes. It can be found that the functional form of heat flux produces few effects on the estimation accuracy and efficiency, which demonstrates the wide applicability of DFIM for reconstructing various heat fluxes of participating medium.

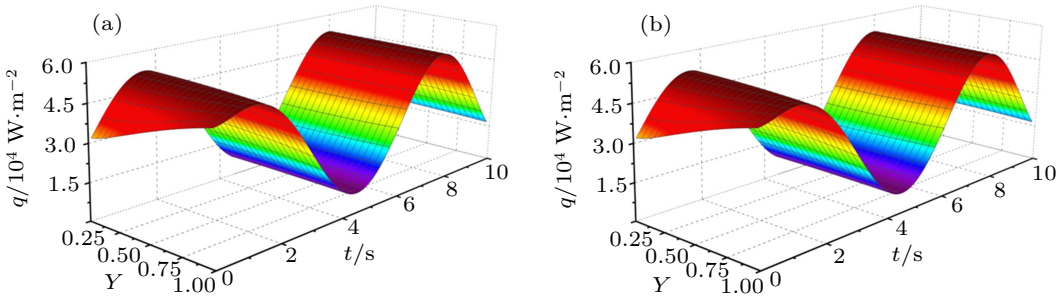


Fig. 7. Retrieval results of heat flux Q2. (a) Exact distribution, and (b) reconstruction result.

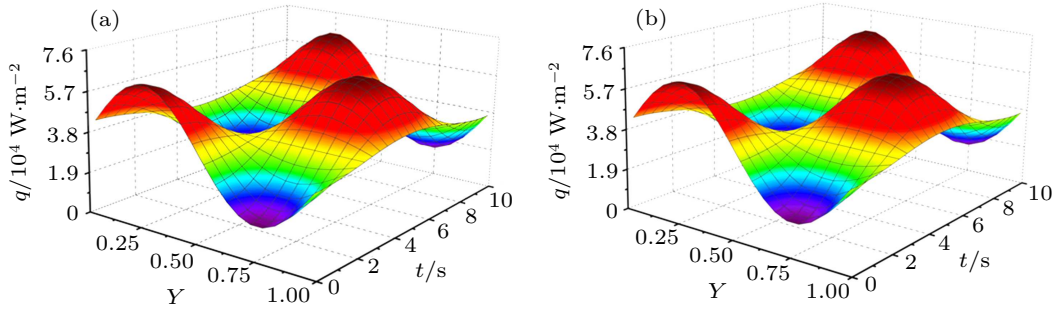


Fig. 8. Retrieval results of heat flux Q3. (a) Exact distribution, and (b) reconstruction result.

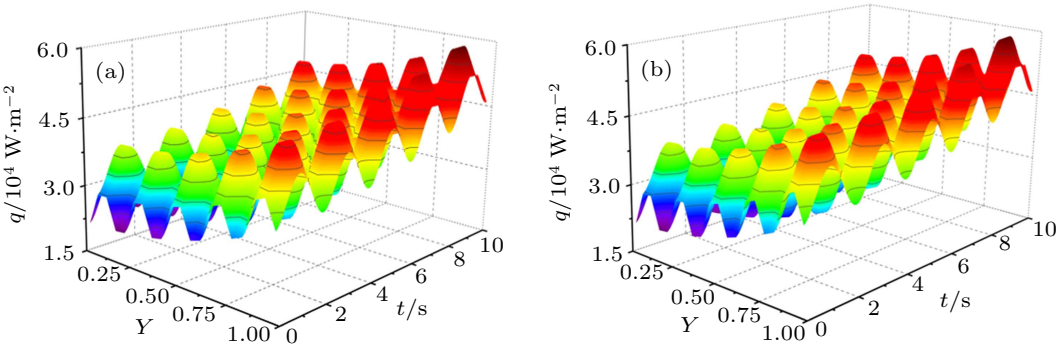


Fig. 9. Retrieval results of heat flux Q4. (a) Exact distribution, and (b) reconstruction result.

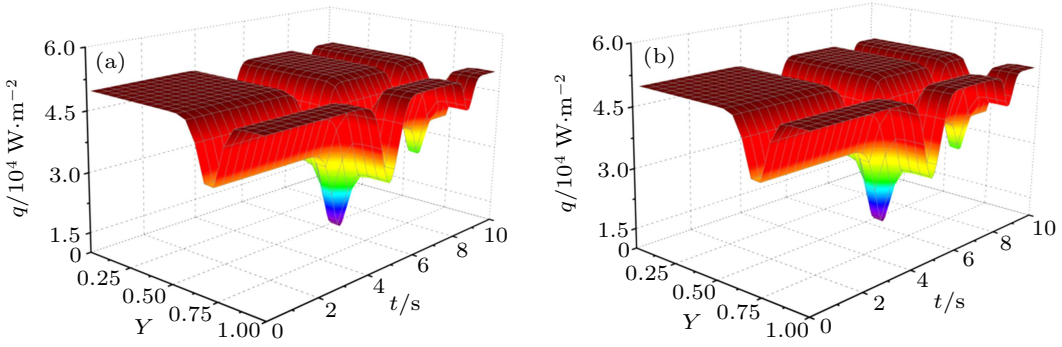


Fig. 10. Retrieval results of heat flux Q5. (a) Exact distribution, and (b) reconstruction result.

Table 4. Reconstruction results of different kinds of heat fluxes.

Heat flux	Average relative error/%	Maximum relative error/%	Iteration number	Computational time/s
Q1	0.0002	0.0092	46	921.1
Q2	0.0002	0.0099	46	922.7
Q3	0.0001	0.0028	45	919.8
Q4	0.0001	0.0030	46	922.3
Q5	0.0001	0.0075	46	923.9

4.3. Effect of initial guess

The reconstruction task starts with an initial guess, and thereby the initial heat flux distribution has a direct effect on the optimization process. Uniform heat flux distributions are employed as initial solutions. The reconstruction results for different initial guessed values are shown in Table 5. The unknown transient heat flux can be precisely recovered by the DFIM. The reconstruction accuracy and computational time for different initial guesses are close. Hence, the initial guess has few effects on the reconstruction results of DFIM.

Table 5. Reconstruction results for different initial guesses.

Initial guess/W·m^{-2}	Average relative error/10^{-6}					Computational time/s				
	Q1	Q2	Q3	Q4	Q5	Q1	Q2	Q3	Q4	Q5
0	1.40	1.97	1.07	0.92	0.79	923.2	923.5	921.0	923.0	921.5
5000	1.38	1.96	1.06	0.93	0.83	921.5	926.4	923.4	921.6	919.4
10000	1.50	1.92	1.05	0.92	0.77	921.1	922.7	919.8	922.3	923.9
30000	1.53	1.90	1.03	0.91	0.83	923.0	921.3	920.1	925.6	921.6
50000	1.99	1.93	1.02	0.91	0.81	922.4	925.4	920.4	922.9	924.1
100000	2.21	2.00	1.16	1.05	0.88	921.6	924.3	922.6	921.7	923.8

4.4. Effect of medium property

The radiative and thermal properties of the medium have critical effects on the heat transfer process, and hence affect the reconstruction result of unknown heat flux. To test the performance of DFIM for reconstructing the time- and space-dependent heat flux in practical engineering fields, two kinds of typical participating engineering materials including ceramic and glass are considered. The main physical parameters of ceramic and glass are illustrated in Table 6.

The medium size and ambient condition are set as same as those in Subsection 4.1. The heat flux Q3 is used as the exact parameters, and the DFIM is applied to solve the optimization task. As shown in Fig. 11, the unknown heat flux irradiated on the surface of ceramic and glass can be precisely recovered. The maximum reconstruction error is less than 0.1%, which illustrates the excellent performance of DFIM for reconstructing the time- and space-dependent heat flux of different kinds of participating media.

Table 6. Parameter of ceramic and glass.[1]

	ρ/kg·m^{-3}	c_p/J·kg^{-1}·K^{-1}	λ/W·m^{-1}·K^{-1}	κ_a/m^{-1}	κ_s/m^{-1}	n
Ceramic	5600	456	1.4	300	12000	1.8
Glass	2219	840	1.025	1244	0	1.4

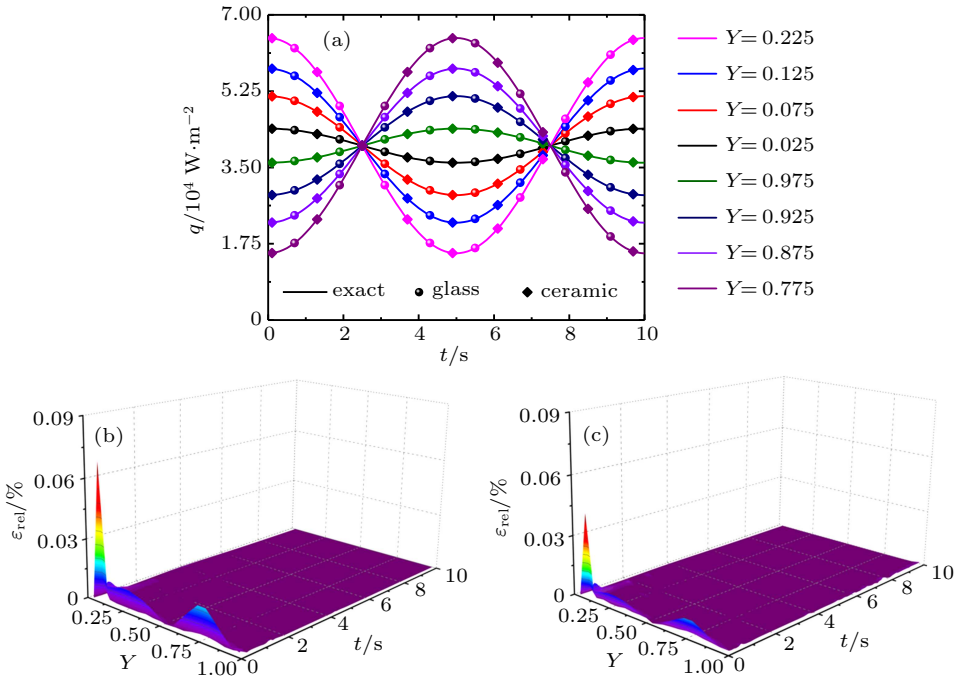


Fig. 11. Reconstruction results of Q3 in ceramic and glass industries. (a) Exact and reconstructed heat fluxes, (b) relative error distribution of ceramic, and (c) relative error distribution of glass.

4.5. Effect of measurement error

Measurement error is inevitable in practical engineering applications. Hence, the effect of measurement error on reconstruction results is studied. Random standard deviations are added to measurement signals. The relative error of retrieval result significantly increases with the increment of measurement error (see Table 7). Meanwhile, it can be seen that measurement errors have few effects on the reconstruction time. Although the measurement error is increased to 1.0, the average relative error is only 2.09 %, and the heat flux distribution can be accurately determined (see Fig. 12). Thus, the DFIM is robust to reconstruct the time- and space-dependent heat flux of participating medium even with noisy data.

Table 7. Retrieval relative errors for different measurement errors.

Measurement error	Average relative error/%	Maximum relative error/%	Computational time/s
0.01	0.0203	0.1560	923.1
0.05	0.1062	0.6897	921.9
0.1	0.2115	1.3735	922.1
0.5	1.0208	6.9042	919.6
1.0	2.0916	12.2036	921.5

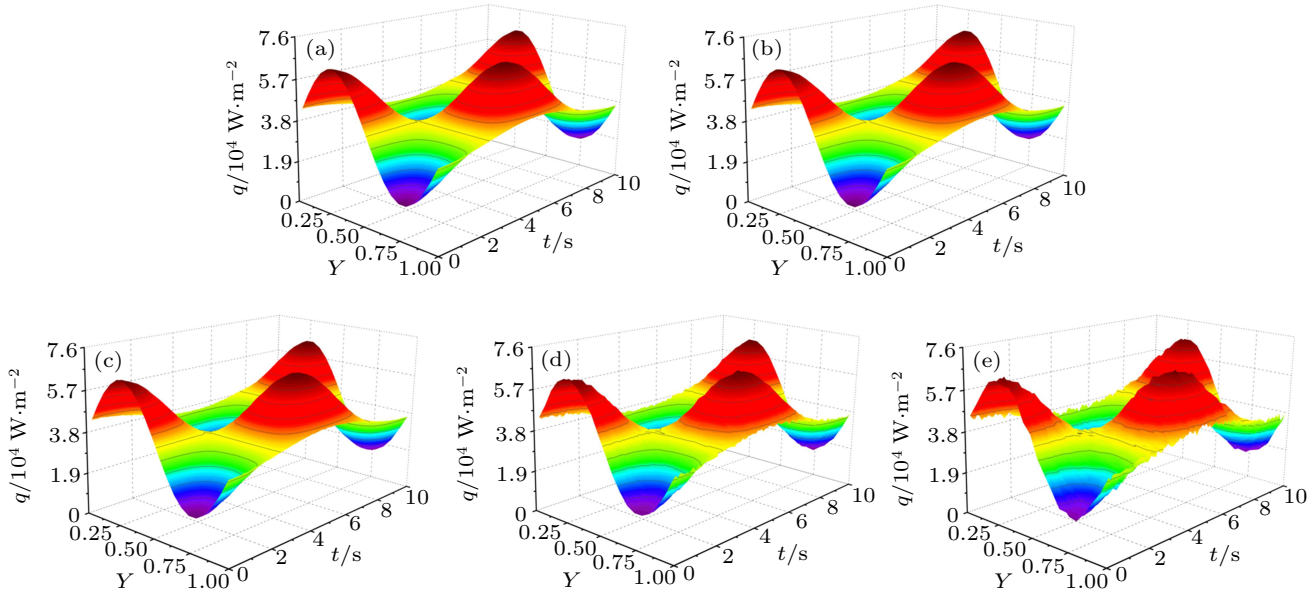


Fig. 12. Reconstruction results of heat flux Q3 for different measurement errors. (a) $\sigma = 0.01$, (b) $\sigma = 0.05$, (c) $\sigma = 0.1$, (d) $\sigma = 0.5$, and (e) $\sigma = 1.0$.

5. Conclusions

In the present work, the time- and space-dependent heat flux of 2D participating medium is reconstructed by using the DFIM. The coupled radiative and conductive model is employed as forward problem to describe the heat transfer process in the medium, which is solved by the FVM–DOM. The temperature distribution on the left surface of the medium is used as measurement signals. The reconstruction of surface heat flux is formulated as an inverse problem. The DFIM is applied to minimize the objective function, through which the unknown incident heat flux is recovered. Meanwhile, the effects of heat flux form, initial guess, medium property, and measurement error on reconstruction results are investigated. The following conclusions can be drawn:

(i) The time- and space-dependent heat flux of participating medium can be precisely reconstructed using DFIM, even with measurement errors.

(ii) The present DFIM is more accurate and efficient in reconstructing the time- and space-dependent heat flux of participating medium than other optimization techniques.

(iii) The functional form of incident heat flux produces few effects on the reconstruction accuracy and efficiency of DFIM.

(iv) The DFIM is effective for different kinds of participating media.

References

[1] Wen S, Qi H, Ren Y T, Sun J P and Ruan L M 2017 *Int. J. Heat Mass Transfer* **111** 582
[2] Dusserre G, Dour G and Bernhart G 2009 *Int. J. Therm. Sci.* **48** 428
[3] Niu C Y, Qi H, Huang X, Wang W, Ruan L M and Tan H P 2015 *Chin. Phys. B* **24** 114401
[4] Liu G N and Liu D 2018 *Chin. Phys. B* **27** 054401
[5] Jalali A, Ayani M B and Baghban M 2014 *J. Therm. Biol.* **45** 37
[6] Yang Y C, Lee H L, Chang W J and Chen W L 2017 *Comput. Methods Biomech. Biomed. Eng.* **20** 446
[7] Zhou S X 2003 *J. Mater. Process. Technol.* **134** 338
[8] Yadav V, Singh A K and Dixit U S 2015 *Int. J. Mech. Sci.* **96–97** 182
[9] Gao J M, Li W, Xia Z W, Pan Y D, Lu J, Yi P and Liu Y 2013 *Chin. Phys. B* **22** 015202
[10] Xia L L 2011 *Chin. Phys. Lett.* **28** 120202
[11] Bose D, White T, Mahzari M and Edquist K 2014 *J. Spacecr. Rockets* **51** 1174
[12] Yan B, Huang S X and Feng J 2018 *Acta Phys. Sin.* **67** 199201 (in Chinese)
[13] Wen S, Qi H, Wang Y F, Ren Y T, Wei L Y and Ruan L M 2020 *Sci. China: Technol. Sci.* **63** 422

[14] Gifford A R, Hubble D O, Pullins C A, Diller T E and Huxtable S T 2010 *J. Thermophys. Heat Transfer* **24** 69

[15] Ozisik M N and Orlande H R B 2000 *Inverse heat transfer* (New York: Taylor & Francis)

[16] Wang Q H, Li Z H, Lai J C and He A Z 2007 *Chin. Phys. Lett.* **24** 1076

[17] Cui K and Yang G W 2005 *Chin. Phys. Lett.* **22** 2738

[18] Xue Q 2018 *Chin. Phys. B* **27** 100203

[19] Qi H, Niu C Y, Gong S, Ren Y T and Ruan L M 2015 *Int. J. Heat Mass Transfer* **83** 428

[20] Qi H, Sun S C, He Z Z, Ruan S T, Ruan L M and Tan H P 2016 *Inverse geometry design of radiative enclosures using particle swarm optimization algorithms* (Rijeka: InTechOpen)

[21] Qi H, Zhao F Z, Ren Y T, Qiao Y B, Wei L Y, Sadaf A I and Ruan L M 2018 *J. Quant. Spectrosc. Radiat. Transfer* **222–223** 1

[22] Li B H and Lu M 2015 *J. Univ. Shanghai Sci. Technol.* **37** 225

[23] Chopade R P, Mohan V, Mayank R, Uppaluri R V S and Mishra S C 2013 *Numer. Heat Transfer, Part A* **63** 373

[24] Chen Z J and Zhang S Y 2010 *Chin. Phys. Lett.* **27** 026502

[25] Sun S C, Qi H, Zhao F Z, Ruan L M and Li B X 2016 *Appl. Therm. Eng.* **98** 1104

[26] He Z Z, Liang D, Mao J K and Han X S 2018 *Chin. Phys. B* **27** 059101

[27] Sun S C, Qi H, Ren Y T, Yu X Y and Ruan L M 2017 *Int. Commun. Heat Mass Transfer* **87** 132

[28] Sun S C, Qi H, Sun J P, Ren Y T and Ruan L M 2017 *Int. J. Therm. Sci.* **120** 121

[29] Qiao Y B, Qi H, Zhao F Z and Ruan L M 2016 *Chin. Phys. B* **27** 120201

[30] Wang Y and Zhao X F. 2019 *Chin. Phys. B* **28** 104301

[31] Yang Y C and Chen W L 2011 *Appl. Therm. Eng.* **31** 2439

[32] Zhu Y H, Liu B, Jiang P X, Fu T R and Lei Y T 2017 *J. Thermophys. Heat Transfer* **31** 205

[33] Cui M, Yang K, Xu X L, Wang S D and Gao X W 2016 *Int. J. Heat Mass Transfer* **97** 908

[34] Sun S C, Wang G J, Chen H and Zhang D Q 2019 *Int. J. Heat Mass Transfer* **134** 574

[35] Zadeh L A 1965 *Inform. Contr.* **8** 338

[36] Wang G J, Wan S B, Chen H, Lv C and Zhang D Q 2017 *Int. J. Heat Mass Transfer* **109** 302

[37] Chen H, Cao D M, Wang G J, Wan S B and Li Y H 2016 *Int. J. Therm. Sci.* **106** 112

[38] Sun S C, Wang G J and Chen H 2020 *Int. J. Therm. Sci.* **149** 106216

[39] Modest M F 2003 *Radiative heat transfer*, 2nd edn. (New York: McGraw-Hill)

[40] Mishra S C, Kumar T B P and Mondal B 2008 *Numer. Heat Transfer A* **54** 798

[41] Sargolzaei J, Khoshnoodi M, Saghatoleslami N and Mousavi M 2008 *Appl. Soft. Comput.* **8** 456

[42] van Broekhoven E and de Baets B 2006 *Fuzzy Set. Syst.* **157** 904